Mechanisms of RALF peptide perception by a heterotypic receptor complex

Xiao, Yu ; Stegmann, Martin ; Han, Zhifu ; DeFalco, Thomas A ; Parys, Katarzyna ; Xu, Li ; Belkhadir, Youssef ; Zipfel, Cyril ; Chai, Jijie

Abstract: Receptor kinases of the Catharanthus roseus RLK1-like (CrRLK1L) family have emerged as important regulators of plant reproduction, growth and responses to the environment1. Endogenous RAPID ALKALINIZATION FACTOR (RALF) peptides2 have previously been proposed as ligands for several members of the CrRLK1L family1. However, the mechanistic basis of this perception is unknown. Here we report that RALF23 induces a complex between the CrRLK1L FERONIA (FER) and LORELEI (LRE)-LIKE GLYCOSYLPHOSPHATIDYLINOSITOL (GPI)-ANCHORED PROTEIN 1 (LLG1) to regulate immune signalling. Structural and biochemical data indicate that LLG1 (which is genetically important for RALF23 responses) and the related LLG2 directly bind RALF23 to nucleate the assembly of RALF23–LLG1–FER and RALF23–LLG2–FER heterocomplexes, respectively. A conserved N-terminal region of RALF23 is sufficient for the biochemical recognition of RALF23 by LLG1, LLG2 or LLG3, and binding assays suggest that other RALF peptides that share this conserved N-terminal region may be perceived by LLG proteins in a similar manner. Structural data also show that RALF23 recognition is governed by the conformationally flexible C-terminal sides of LLG1, LLG2 and LLG3. Our work reveals a mechanism of peptide perception in plants by GPI-anchored proteins that act together with a phylogenetically unrelated receptor kinase. This provides a molecular framework for understanding how diverse RALF peptides may regulate multiple processes, through perception by distinct heterocomplexes of CrRLK1L receptor kinases and GPI-anchored proteins of the LRE and LLG family. This project has received funding from the European Research Council (ERC) under the European Union's Horizon 2020 research and innovation programme (grant agreement No 773153)

DOI: https://doi.org/10.1038/s41586-019-1409-7

Mechanisms of RALF peptide perception by a heterotypic receptor complex

Yu Xiao[1,*], Martin Stegmann[2,7*], Zhifu Han[1,*], Thomas A. DeFalco[2,3], Katarzyna Parys[4], Li Xu[1], Youssef Belkhadir[4], Cyril Zipfel[2,3#] and Jijie Chai[1,5,6#]

[1]School of Life Sciences, Innovation Center for Structural Biology, Tsinghua-Peking Joint Center for Life Sciences, Tsinghua University, Beijing, 100084, China.

[2]The Sainsbury Laboratory, University of East Anglia, Norwich Research Park, Norwich, NR4 7UH, UK.

[3]Institute of Plant and Microbial Biology and Zurich-Basel Plant Science Center, University of Zurich, CH-8008 Zurich, Switzerland.

[4]Gregor Mendel Institute (GMI), Austrian Academy of Sciences, Vienna Biocenter (VBC), 1030 Vienna, Austria.

[5]Max-Planck Institute for Plant Breeding Research, 50829 Cologne, Germany.

[6]Institute of Biochemistry, University of Cologne, 50674 Cologne, Germany.

[7]Chair of Phytopathology, Technical University of Munich, School of Life Sciences Weihenstephan, 85354 Freising-Weihenstephan, Germany.

*Equal contributions.

[#]Correspondence: Jijie Chai, chaijj@mail.tsinghua.edu.cn; Cyril Zipfel, cyril.zipfel@botinst.uzh.ch

Summary

Receptor kinases (RKs) of the *Catharantus roseus* RLK1-like (CrRLK1L) family have emerged as important regulators of plant reproduction, growth and responses to the environment[1]. Endogenous RAPID ALKALINIZATION FACTOR (RALF) peptides[2] have been proposed as ligands for several CrRLK1L members[1]. The mechanistic basis of this perception, however, is unknown. Here, we report that RALF23 induces a complex between the CrRLK1L FERONIA (FER) and LORELEI (LRE)-LIKE GLYCOSYLPHOSPHATIDYLINOSITOL (GPI)-ANCHORED PROTEIN 1 (LLG1) to regulate immune signalling. Structural and biochemical data indicate that LLG1, which is genetically important for RALF23 responses, or the related LLG2, directly binds RALF23 to nucleate the assembly of a RALF23-LLG1/2-FER heterocomplex. A conserved N-terminal region of RALF23 is sufficient for its biochemical recognition by LLG1/2/3, and binding assays suggest other RALFs sharing this conserved N-terminal region may be perceived in a similar manner. Structural data also show that RALF23 recognition is governed by the conformationally flexible C-terminal sides of LLG1/2/3. Our work reveals an unexpected mechanism of plant peptide perception by GPI-anchored proteins in concert with a phylogenetically-unrelated RK, which provides a molecular framework to understand how diverse RALF peptides may regulate multiple processes through perception by distinct heterocomplexes between CrRLK1L RKs and GPI-anchored proteins of the LRE/LLG family.

Plant RKs play important roles in sensing intrinsic and extrinsic cues to regulate cellular activities. The CrRLK1L subfamily of RKs comprises 17 members in *Arabidopsis thaliana* (hereafter, Arabidopsis) with two tandem malectin-like modules in their extracellular domains (ECDs)[1]. FER is the best studied CrRLK1L and regulates many aspects of the plant life including growth and immunity[3-7].

Plant RALF peptides were recently proposed as CrRLK1L ligands[1]. For example, RALF1 and RALF23 bind to FER to regulate root growth and immunity, respectively[4,5], while RALF4 and RALF19 bind to the CrRLK1Ls ANXUR (ANX) 1/2 and BUDDHA PAPER SEAL (BUPS) 1/2 to control pollen tube growth and integrity[8]. Yet, the molecular basis of RALF perception is still unknown.

The GPI-anchored protein LRE and its homolog LLG1 are important components of FER-mediated signalling[9-11]. In Arabidopsis, LRE and its three homologs LLG1, 2 and 3 have differential expression patterns[11]. Like *FER*, *LLG1* is strongly expressed in vegetative tissues, while *LLG2* and *LLG3* are predominantly expressed in reproductive tissues (Extended Data Fig. 1a). Both *FER* and *LLG1* regulate immune signalling triggered by the bacterial pathogen-associated molecular patterns (PAMPs) flg22 and elf18[5,12] (Fig. 1a, Extended Data Fig. 1b). Like *FER*[5], *LLG1* regulated flg22-induced FLAGELLIN-SENSING 2 (FLS2) - BRASSINOSTEROID INSENSITIVE 1-ASSOCIATED KINASE 1 (BAK1) interaction (Extended Data Fig. 1c), in contrast to what was previously reported when *FLS2* was overexpressed[12]. As previously shown for *fer-2*[5], *llg1*-2 mutant plants were also impaired in RALF23-induced inhibitions of elf18-induced reactive oxygen species (ROS) production (Fig. 1b) and of seedling growth (Fig. 1c). LLG1 is thus an important component of FER-dependent RALF23 perception in Arabidopsis.

Analytical ultra-centrifugation (AUC) and isothermal titration calorimetry (ITC) assays detected no interaction between FER^{ECD} and LLG1 (Fig. 1d, left panel; Fig. 1e, left panel). Further ITC experiments showed that RALF23 interacted with FER^{ECD}, with a dissociation constant (K_d ~1.52 μM) (Fig. 1e, middle panel), consistent with previously reported binding affinities[5]. Interestingly, the assays demonstrated a direct

RALF23 interaction with LLG1 (K_d ~4.95 μM) (Fig. 1e, right panel), LLG2 or LLG3 (Extended Data Fig. 2a,b). Furthermore, AUC assays showed that addition of RALF23 to FER^{ECD} and LLG1 resulted in formation of a protein complex with a molecular weight of ~80 kD (Fig. 1d, right panel), equivalent to monomeric RALF23-LLG1-FER^{ECD}. Similarly, RALF23 also induced a complex between FER^{ECD} and LLG2 or LLG3 (Extended Data Fig. 2c,d). Co-immunoprecipitation experiments further confirmed that exogenous RALF23 treatment induced a strong LLG1-FER complex in Arabidopsis (Fig. 1f, Extended Data Fig. 2e). Together, these data suggest that RALF23 binding induces LLGs heterodimerization with FER^{ECD}.

We next solved the crystal structures of apo-FER^{ECD}, apo-$ANX1^{ECD}$, apo-$ANX2^{ECD}$, apo-LLG1, and RALF23-LLG2-FER^{ECD} (Fig. 2a, Extended Data Fig. 3a-c and Table 1). We were unfortunately unable to solve a crystal structure of RALF23-LLG1-FER^{ECD}. Electron density of FER and LLG2 (Extended Data Fig. 3d,e) suggests that both proteins were glycosylated at sites outside the protein-protein interaction interfaces (Extended Data Fig. 3f).The structure of FER^{ECD} resembles those of $ANX1^{ECD}$, $ANX2^{ECD}$ [13,14] (Extended Data Fig. 4a) and *Xenopus laevis* malectin protein[15] (Extended Data Fig. 4b); however, FER^{ECD} lacks the saccharide-binding site of malectin (Extended Data Fig. 4b,c) similar to $ANX1^{ECD}$ and $ANX2^{ECD}$ [13,14]. Crystal structural comparison showed that no striking conformational changes occur to FER^{ECD} following interaction with RALF23 and LLG2 (Extended Data Fig. 4d). The structure of LLG2 is mainly helical and the N-terminal side of RALF23 forms an α-helix interacting with both LLG2 and FER^{ECD} (Fig. 2a). The C-terminal side of RALF23 is absent in the complex structure, perhaps due to its flexibility in crystals.

In the RALF23-LLG2-FER^{ECD} structure, the N-terminal helix of RALF23 binds to a large surface groove on LLG2 (Extended Data Fig. 4e,f). The conserved 'YISY' motif essential for RALF1-induced alkalinization[16], forms extensive interactions with LLG2 via a combination of hydrophobic and polar contacts (Fig. 2b). FER^{ECD} interacts with both RALF23 and LLG2, with α-helix3 of FER^{ECD} packing against α-helix5 and the loop region N-terminal to α-helix2 of LLG2 and the loop region N-terminal to β-sheet16 of FER^{ECD} interacting with α-helix2 of LLG2 and RALF23 (Fig. 2c and Extended Data Figs 4g,5).

The extensive interactions of the N-terminal 14 residues (4-17) of RALF23 with LLG2 (Fig. 2b) suggest that this RALF23 region may be sufficient for interaction with LLGs. Accordingly, an N-terminal fragment of RALF23 containing residues 1-17 (RALF23-17mer; $RALF23^{N}$) interacted with LLG1/2/3 but not with FER^{ECD} in ITC and surface plasmon resonance (SPR) assays (Extended Data Fig. 6a,b). The RALF23-17mer induced LLG1/2/3-FER^{ECD} interaction, albeit with a lower activity than full-length RALF23 (Extended Data Fig. 6c,d). Although protein folding efficiency might contribute to the affinity differences, these results suggest a role of the RALF23 C-terminus (residues 18-50; $RALF23^{C}$) in RALF23-induced LLGs-FER complexes. Indeed, our microscale thermophoresis (MST) assays showed that $RALF23^{C}$ but not $RALF23^{N}$ interacted with FER^{ECD} with Kd ~1.01 μM, compared to ~0.31 μM for full-length RALF23 (Fig. 2d). This is consistent with a recent study suggesting that RALF1 C-terminus interacts with FER[17]. In contrast, $RALF23^{C}$ displayed no interaction with LLG1/2/3 (Extended Data Fig. 6e). Taken together, these data (Table 1) indicate that $RALF23^{N}$ is sufficient to nucleate an LLG-FER^{ECD} complex further reinforced by $RALF23^{C}$. Consistently, neither $RALF23^{C}$ nor $RALF23^{N}$ alone induced seedling growth inhibition (Extended Data Fig. 7a).

The N-terminal 14 residues (4-17) of RALF23 are conserved in related RALFs (named subfamily 1; Extended Data Fig. 7b), suggesting that they may also interact with LLGs. Indeed, N-terminal fragments of RALF1/14/19/24/27/31/34 displayed affinities with LLG2 when assayed by ITC, but not the subfamily 2 RALFs 11/12/13 or 21 (Table 2, Extended Data Fig. 7c-f). Furthermore, our AUC results showed that some members of subfamily 1, including RALF1, induced LLG1 interaction with FER^{ECD} *in vitro* (Extended Data Fig. 8a). Collectively, our *in vitro* data suggest that LLGs can bind multiple RALFs. However, the fact that *fer* and *llg1* mutants phenocopied each other[11] (Fig. 1a-c, Extended Data Fig. 1b,c) suggests that LLG1 plays a dominant role in leaf and seedling tissues assayed in our study, consistent with its higher expression there (Extended Data Fig. 1a).

Twelve out of thirteen RALF23-interacting residues of LLG2 are conserved in LLG1, LLG3 and LRE (Extended Data Fig. 8b, blue dots). However, LRE displayed no RALF23-binding affinity (Fig. 3a) and RALF23 failed to induce an LRE-FER^{ECD} complex (Extended Data Fig. 8c). In apo-LLG1, residues 129-138 (Fig. 3b, left panel

in grey) bind to the pocket equivalent to the RALF23-binding groove of LLG2 (Fig. 3b, right panel), suggesting that conformational changes occur to this region of LLG1 for binding to RALF23. Consistently, residues 126-134 of RALF23-bound LLG2 are flexible (Fig. 3b, right panel in grey), whereas the 'KEGKEGLD' fragment flips about 90 degrees compared to that of apo-LLG1 (Fig. 3c, left panel, framed in blue). Moreover, Leu127 and Glu128 of apo-LLG1 severely clash with RALF23 when apo-LLG1 is aligned with LLG2 in RALF23-LLG2-FER^{ECD} (Fig. 3c, right panel). The 'KEGKEGLD' fragment is conserved among LLG1/2/3 and LRE, except an arginine substitution of the first glycine in LRE (Extended Data Fig. 8b, black dot). This can decrease the conformational flexibility of 'KEGKEGLE/D' provided by the two glycine residues in LLG1/2/3 for RALF23 interaction. Indeed, mutation of the first glycine residue (Gly123) to arginine in LLG1 compromised interaction with RALF23 (Fig. 3a). Conversely, substitution of arginine to glycine at the same position enabled LRE to bind RALF23, albeit with reduced affinity compared to LLG1 (Fig. 3a).

The recently reported *llg1-3* mutant carries a G114R substitution[12]. The corresponding residue in LLG2, Gly109, establishes hydrophobic packing against Ile16 of RALF23 (Fig. 2b). Mutation of this residue to the bulky arginine residue in LLG1 significantly reduced LLG1 interaction with RALF23 *in vitro* (Table 3, Extended Data Fig. 9a). Importantly, *llg1-3* was impaired in RALF23-triggered seedling growth inhibition (Fig. 4a), confirming our structural data *in vivo*.

Supporting our structural observations, the GST-RALF23-17mer (GST-17mer) interacted with LLG1/2/3 (Fig. 4b) in pull-down assays. In contrast, mutations of critical residues of RALF23, LLG2 at the RALF23-LLG2 interface (Fig. 2b) or the LLG2 equivalent residues of LLG1 resulted in no detectable RALF23 interaction with LLG2 or LLG1, respectively (Fig. 4c, Extended Data Fig. 9b). Similarly, mutations of residues in FER^{ECD} directly involved in interaction with RALF23 or LLG2 (or LLG1 based on conservation of these LLG2 residues) significantly reduced FER^{ECD} binding to the pre-formed RALF23-17mer-LLG1/2 complex or FER^{ECD} with RALF23-17mer-LLG1 N118Y complex tested by ITC (Table 4, Extended Data Fig. 9c-e). Further supporting our structural observations, RALF23 induced inhibitions of elf18-induced ROS production and seedling growth (Fig. 1b, c) were impaired by mutations of residues (RALF23 I6A, I6Y, L11Y and N14A) critical for interaction with LLG1 (Fig. 4d, e). Furthermore, when expressed in the *fer-4* background, both FER G257A and FER

N303Y were hyposensitive to RALF23-induced seedling growth inhibition, compared to WT FER (Fig. 4f), despite their comparable expression levels (Extended Data Fig. 9f). Finally, upon transient expression in *Nicotiana benthamiana*, RALF23 induced LLG1-FER interaction while LLG1 N91A, T99R, A117Y and N118Y did not (Extended Data Fig. 9g), providing additional support for conclusions extrapolated from the LLG2-containing structure.

Here we show that direct RALF23 recognition by LLG1 results in the nucleation of a ternary complex with FER, revealing a novel type of heteromeric receptor complex for perception of plant peptides. The N-terminal 'YISY' motif required for RALF23-induced LLG1-FER heteromerization, immunity and growth inhibition is conserved in a subfamily of RALFs. Our biochemical data suggest the existence of multiple RALF-LLG-FER^{ECD} complexes. Although the biological functions for most of them remain largely unknown, recognition of multiple, potentially cell and/or tissue-specific 'YISY'-containing RALFs by FER via distinct LLGs is consistent with the multitasking role of FER[1]. FER-LLG1 interaction induced by exogenous RALF23 peptide in Arabidopsis (Fig. 1f) suggests a plasma membrane localization of the complex for signaling. Additional signaling components such as RKs might also be recruited to the complex as illustrated for ANX1/2 and BUPS1/2[8], possibly via the RALF C-terminus similar to what has been observed with flg22[18,19]. Although this hypothesis remains to be further tested, recent data suggest that RALF perception and CrRLK1L-controlled processes also involve cell wall-localized leucine-rich-repeat extensin proteins (LRXs)[6,20-22], raising the possibility that they participate in a supramolecular complex required for RALF signaling[23].

References

1 Franck, C. M., Westermann, J. & Boisson-Dernier, A. Plant Malectin-Like Receptor Kinases: From Cell Wall Integrity to Immunity and Beyond. *Annu. Rev. Plant Biol.* **69**, 301-328 (2018).

2 Pearce, G., Moura, D. S., Stratmann, J. & Ryan, C. A., Jr. RALF, a 5-kDa ubiquitous polypeptide in plants, arrests root growth and development. *Proc. Natl. Acad. Sci. U. S. A.* **98**, 12843-12847 (2001).

3 Escobar-Restrepo, J. M. *et al.* The FERONIA receptor-like kinase mediates male-female interactions during pollen tube reception. *Science* **317**, 656-660 (2007).

4 Haruta, M., Sabat, G., Stecker, K., Minkoff, B. B. & Sussman, M. R. A peptide hormone and its receptor protein kinase regulate plant cell expansion. *Science* **343**, 408-411 (2014).

5 Stegmann, M. *et al.* The receptor kinase FER is a RALF-regulated scaffold controlling plant immune signaling. *Science* **355**, 287-289 (2017).

6 Zhao, C. *et al.* Leucine-rich repeat extensin proteins regulate plant salt tolerance in Arabidopsis. *Proc. Natl. Acad. Sci. U. S. A.* **115**, 13123-13128 (2018).
7 Feng, W. *et al.* The FERONIA Receptor Kinase Maintains Cell-Wall Integrity during Salt Stress through Ca(2+) Signaling. *Curr. Biol.* **28**, 666-675 e665 (2018).
8 Ge, Z. *et al.* Arabidopsis pollen tube integrity and sperm release are regulated by RALF-mediated signaling. *Science* **358**, 1596-1600 (2017).
9 Capron, A. *et al.* Maternal control of male-gamete delivery in Arabidopsis involves a putative GPI-anchored protein encoded by the LORELEI gene. *Plant Cell* **20**, 3038-3049 (2008).
10 Liu, X. *et al.* The Role of LORELEI in Pollen Tube Reception at the Interface of the Synergid Cell and Pollen Tube Requires the Modified Eight-Cysteine Motif and the Receptor-Like Kinase FERONIA. *Plant Cell* **28**, 1035-1052 (2016).
11 Li, C. *et al.* Glycosylphosphatidylinositol-anchored proteins as chaperones and co-receptors for FERONIA receptor kinase signaling in Arabidopsis. *Elife* **4** (2015).
12 Shen, Q., Bourdais, G., Pan, H., Robatzek, S. & Tang, D. Arabidopsis glycosylphosphatidylinositol-anchored protein LLG1 associates with and modulates FLS2 to regulate innate immunity. *Proc. Natl. Acad. Sci. U. S. A.* **114**, 5749-5754 (2017).
13 Du, S., Qu, L. J. & Xiao, J. Crystal structures of the extracellular domains of the CrRLK1L receptor-like kinases ANXUR1 and ANXUR2. *Protein Sci.* **27**, 886-892 (2018).
14 Moussu, S., Augustin, S., Roman, A. O., Broyart, C. & Santiago, J. Crystal structures of two tandem malectin-like receptor kinases involved in plant reproduction. *Acta crystallographica. Section D, Structural biology* **74**, 671-680 (2018).
15 Schallus, T. *et al.* Malectin: a novel carbohydrate-binding protein of the endoplasmic reticulum and a candidate player in the early steps of protein N-glycosylation. *Mol. Biol. Cell* **19**, 3404-3414 (2008).
16 Pearce, G., Yamaguchi, Y., Munske, G. & Ryan, C. A. Structure-activity studies of RALF, Rapid Alkalinization Factor, reveal an essential--YISY--motif. *Peptides* **31**, 1973-1977 (2010).
17 Liu, P., Haruta, M., Minkoff, B. B. & Sussman, M. R. Probing a Plant Plasma Membrane Receptor Kinase's Three-Dimensional Structure Using Mass Spectrometry-Based Protein Footprinting. *Biochemistry* **57**, 5159-5168 (2018).
18 Chinchilla, D., Bauer, Z., Regenass, M., Boller, T. & Felix, G. The Arabidopsis receptor kinase FLS2 binds flg22 and determines the specificity of flagellin perception. *Plant Cell* **18**, 465-476 (2006).
19 Sun, Y. *et al.* Structural basis for flg22-induced activation of the Arabidopsis FLS2-BAK1 immune complex. *Science* **342**, 624-628 (2013).
20 Mecchia, M. A. *et al.* RALF4/19 peptides interact with LRX proteins to control pollen tube growth in Arabidopsis. *Science* **358**, 1600-1603 (2017).
21 Fabrice, T. N. *et al.* LRX Proteins Play a Crucial Role in Pollen Grain and Pollen Tube Cell Wall Development. *Plant Physiol.* **176**, 1981-1992 (2018).
22 Sede, A. R. *et al.* Arabidopsis pollen extensins LRX are required for cell wall integrity during pollen tube growth. *FEBS Lett.* **592**, 233-243 (2018).
23 Stegmann, M. & Zipfel, C. Complex regulation of plant sex by peptides. *Science* **358**, 1544-1545 (2017).

Figure legends

Figure 1 | *LLG1* is important for RALF23 responses and RALF23 induces LLG1-FER heterodimerization.

a Mean values of total reactive oxygen species (ROS) production over 40 min after elicitation with 100 nM elf18 (n=8 +/- SD).

b Mean values of total ROS production over 40 min after elicitation of the indicated genotypes with 100 nM elf18 (2 mM MES-KOH pH 5.8) or co-treatment with 1 µM RALF23 (n=16 +/- SD). One-way ANOVA ($p < 0.0001$).

c Five day-old seedlings were treated with 1 µM RALF23 for 7 days.. Shown is the mean of relative fresh weight compared to the MS control (n=16 +/-SD). One-way ANOVA ($p<0.0001$).

d Analyses of LLG1, FER^{ECD} and LLG1+FER^{ECD} (left), and LLG1+FER^{ECD} and RALF23+LLG1+FER^{ECD} (right) proteins by sedimentation-velocity analytical ultracentrifugation (SV-AUC). The peak sedimentation coefficients of the proteins in SV-AUC are indicated.

e Quantification of binding affinities by isothermal titration calorimetry (ITC) assays. Left panels: LLG1 was titrated into FER^{ECD}. Middle and right panels: RALF23 peptide was titrated into FER^{ECD} or LLG1. The binding constants (K_d values ± fitting errors) and stoichiometries (n) are indicated. n.d.: no detectable binding.

f *llg1-3* 35S::YFP-LLG1 seedlings were treated with or without 1 µM RALF23 before immunoprecipitation. See Supplementary Fig. 1 for western blot source data. For **a-f**, experiments were repeated at least three times with similar results. For **a-c**, letters indicate the result of a post hoc turkey test. Columns with same letters are statistically indistinguishable (>95% confidence). See supplementary statistical information for multiple comparison p-values.

Figure 2 | The conserved N-terminal region of RALF23 is sufficient to induce LLG1/2/3 interaction with FER, which is reinforced by the C-terminal part of RALF23.

a Overall structure of the RALF23-LLG2-FER^{ECD} complex in two orientations. FER^{ECD}, LLG2 and RALF23 shown in cartoon and surface are coloured with cyan, purple and brown, respectively. Important secondary structures are labelled. “N” and “C” represent N- and C-termini. “α” and “β” represent α-helices and β-sheets.

b Detailed view of LLG2-RALF23 interactions. Dashed lines indicate polar interactions. Left panel: RALF23 (residues 4-10 containing ‘YISY’ motif) interacts with LLG2. Right panel: RALF23 (residues 11-17) interacts with LLG2.

c Detailed view of FER^{ECD} interactions with LLG2 and RALF23. Left panel: α3 of FER^{ECD} packing against α5 and the loop region N-terminal to α2 of LLG2. Right panel: the loop region N-terminal to β16 of FER^{ECD} interacting with the α2 of LLG2 and RALF23. Dashed lines indicate polar interactions.

d Quantification of binding affinity between fluorescently labelled FER^{ECD} and RALF23, $RALF23^{N}$ (residues 1-17) or $RALF23^{C}$ (residues 18-50) by MST. Data points indicate the difference in normalized fluorescence [‰] generated by FER^{ECD} or liganded FER^{ECD}, and curves indicate the calculated fits. Error bars represent standard error of 3 independent measurements. Mean values of binding affinity are shown in bold. The experiments were repeated three times with similar results.

Figure 3 | The conformationally flexible regions in LLG/LRE determine their interaction with RALF23.

a Quantification of binding affinities of RALF23 with LRE, LLG1 G123R, LRE R120G by ITC. The calculated n and K_d values are indicated. The assays were performed three times independently with similar results as described in Fig. 1**e**.

b Structural comparison between apo-LLG1 (left) and RALF23-bound LLG2 (right), shown in the same orientation.

c Left panel: structural superposition of apo-LLG1 and RALF23-LLG2. Right panel: Residues with severe clashes between apo-LLG1 and RALF23 are highlighted within the blue dashed frame and labelled. For **b-c**, the disulfides are shown in yellow. Colour codes and related residues are indicated

Figure 4 | Mutagenesis-based analysis of the RALF23-LLG1-FER^{ECD} complex.

a Seedlings were treated with 1 µM RALF23 for 7 days. Shown is the mean of relative fresh weight compared to MS control (n=8 +/-SD). One-way ANOVA ($p<0.0001$).

b Purified LLG1/2/3 were incubated with GS4B resin bound GST-RALF23-17mer (GST-17mer). Analysis by SDS-PAGE and Coomassie blue staining.

c Mutagenesis analyses of GST-17mer-LLG1 interaction. Left panel: SDS-PAGE of LLG1 pull-down by WT or GST-17mer mutants. Right panel: SDS-PAGE of WT

or LLG1 mutants pulled down by GST-17mer. For **c** and **d**, see Supplementary Fig. 2 for gel source data.

d ROS burst measured after elicitation of Col-0 leaf discs with 100 nM elf18 or co-treatment with 500 nM RALF23 or variants. Values are means of total photon counts relative to elf18 of four independent experiments. n=159 (no RALF23), 48 ($RALF23^{WT}$), 24 ($RALF23^{I6A}$, $RALF23^{I6Y}$, $RALF23^{L11Y}$, $RALF23^{N14A}$) +/- SD.

e Col-0 seedlings were treated with 500 nM RALF23 or variants for 7 days. Shown is the mean of relative fresh weight compared to MS control of four independent experiments. n=90 (MS), 30($RALF23^{WT}$), 16 ($RALF23^{I6A}$), 28 ($RALF23^{L11Y}$), 30 ($RALF23^{N14A}$) +/- SD. **f** and **g**: One-way ANOVA ($p<0.0001$).

f Five day-old seedlings were treated with 500 nM RALF23 for 7 days. Shown is the mean of relative fresh weight compared to MS control of three independent experiments (n=24) +/- SD. One-way ANOVA ($p<0.0001$). For **a-f**, experiments were repeated three times with similar results. For **a**, **d-f**, letters indicate the result of a post hoc turkey test. Columns with same letters are statistically indistinguishable (>95% confidence). See supplementary statistical information for multiple comparison p-values.

Table 1 | Summary of ITC data for full length or RALF23 variants binding to LLG1/2/3 or FER^{ECD}. Raw data are shown in Fig. **1e** and Extended Data Figs **2a-b, 6b-e.** Similar results were obtained in three independent repeats.

Ligand (syringe) to protein (cell)	RALF23 to LLG1/2/3 / FER^{ECD}	RALF23-17mer to LLG1/2/3 / FER^{ECD}	RALF23 (18-50) to LLG1/2/3
K_d (μM)	4.95 / 0.81 / 3.83 / 1.52	1.30 / 0.21 / 2.28 / n.d.	n.d. / n.d. / n.d.

Ligand (syringe) to protein (cell)	LLG1/2/3 to FER^{ECD}	RALF23-17mer + LLG1/2/3 to FER^{ECD}	RALF23 + LLG1/2/3 to FER^{ECD}
K_d (μM)	n.d. / n.d. / n.d.	4.83 / 9.10 / 9.80	1.53 / 3.21 / 3.83

Table 2 | Summary of ITC data for binding of different N-terminal peptides of RALFs to LLG2. Boundaries of the RALF-derived peptides and raw data are shown in Extended Data Fig. **7c,d,f**. Similar results were obtained in three independent repeats.

Ligand (syringe) to LLG2 (cell)	RALF 1-17mer	RALF1 4-16mer	RALF1 9-18mer	RALF2 3-17mer	RALF2 4-18mer	RALF2 7-15mer	RALF3 1-18mer	RALF3 4-20mer	RALF11/12/ 13-22mer	RALF2 1-16mer
K_d (μM)	11.04	0.27	0.83	0.21	1.85	3.68	2.88	0.34	n.d.	n.d.

Table 3 | ITC result summary: RALF23 interaction with $LLG1^{WT}$/$LLG1^{G114R}$. Raw data are shown in Extended Data Fig. **9a**. Similar results were obtained in three independent repeats.

RALF23 (syringe) to LLG1(cell)	WT	LLG1 G114R
K_d (μM)	4.95	36.1

Table 4 | Summary of ITC results on RALF23-17mer+LLG1 interaction with FER^{WT}/FER^{ECD} mutants. Raw data are shown in Extended Data Fig. **9c**. Similar results were obtained in three independent repeats.

RALF23-17mer+LLG1 (syringe) to FER^{ECD} (cell)	WT	LLG1 N118Y	FER^{ECD} A258Y/I300Y/N303Y/Y304A
K_d (μM)	4.83	n.d.	n.d. / n.d. / n.d. / n.d.

Methods

Synthetic peptides and elicitors

The flg22, elf18, RALF23, RALF23 variants and other RALF peptides (Extended Data Fig. 7c) were synthesized by EZBiolab (United States) or SciLight (China) with purity of >90%. All the peptides were dissolved in sterile pure water for usage.

Protein expression and purification

The extracellular domains of FER (residues 27-447), ANX1 (residues 27-430), ANX2 (residues 28-431), LLG1 (residues 24-152), LLG2 (residues 24-146), LLG3 (residues 24-149), LRE (residues 21-149), synthesized by GENEWIZ (China), were cloned into modified pFastBac vectors, containing an N-terminal hemolin signal peptide and a C-terminal 6×His-tag or a cleavable N-terminal 6×His-SUMO tag using a ligase kit (Sosoo Mix, TsingKe Co, Ltd, China). All the proteins were expressed using the Bac-to-Bac baculovirus expression system (Invitrogen) protocols in High Five cells at 22 °C. One litre of cells (2.0×10^6 cells/mL) was infected with 30 mL recombinant baculovirus. The supernatant was harvested via centrifugation 60 h post-infection. The supernatant was flowed through Ni-NTA (Novagen). Bound proteins were eluted in a buffer containing 25 mM Tris pH8.0, 150 mM NaCl, 250 mM imidazole and further purified by size-exclusion chromatography (Hiload 16/60 Superdex 200 prep grade, GE Healthcare) in a buffer containing 10 mM Bis-Tris pH 6.0, 100 mM NaCl. All the RALF peptides were diluted to a final concentration of 1 mM in a buffer containing 10 mM Bis-Tris pH 6.0, 100 mM NaCl. For RALF23, it was renatured in open 1.5 mL tubes for 12 h at 4°C. To obtain the RALF23- LLG2-FER^{ECD} complex crystals, the purified FER^{ECD}, LLG2 and RALF23 peptide were mixed with a molar ratio of ~1:1:1 and incubated at 4 °C for 30 min. The proteins for the FER^{ECD}, $ANX1^{ECD}$, $ANX2^{ECD}$, LLG1 and RALF23-LLG2-FER^{ECD} mixture were concentrated to about 10 mg mL^{-1} for crystallization.

Crystallization, data collection, structure determination and refinement

Crystallization experiments were performed by hanging-drop vapor-diffusion methods by mixing 1 μL of protein with 1 μL of reservoir solution at 18 °C. Diffraction quality

crystals of FER^{ECD} were obtained in the buffer containing 0.1 M Bis-Tris pH 6.5, 25% w/v Polyethylene glycol 3350. Good quality crystals of $ANX1^{ECD}$ or $ANX2^{ECD}$ were obtained in the buffer containing 0.2 M ammonium acetate, 0.1 M BIS-Tris pH 6.5, 25% w/v Polyethylene glycol 3350, or 0.2 M sodium fluoride, 25% Polyethylene glycol 3350. For LLG1, high quality crystals emerged in the buffer containing 0.1 M Bis-Tris pH 6.5, 28% Polyethylene glycol 2,000. All crystals were flash frozen using the reservoir buffer plus 17% glycerol as the cryoprotectant. Diffraction quality crystals of RALF23-LLG2-FER^{ECD} were obtained in the buffer containing 0.2 M sodium malonate, 25% w/v Polyethylene glycol 3350. All diffraction datasets were collected at Shanghai Synchrotron Radiation Facility (SSRF) on beam line BL17U1 or BL19U using a CCD detector[24]. All data were processed using the HKL2000 software package[25]. Initial phases of $ANX2^{ECD}$ were obtained by platinum-based single-wavelength dispersion (SAD) method using the Pt_2Cl_6-derived $ANX2^{ECD}$ crystals. The crystal structures of FER^{ECD} and $ANX1^{ECD}$ were determined by molecular replacement (MR) with PHASER[26] using the structure of $ANX2^{ECD}$ as the initial searching model. The crystal structure of RALF23-LLG2-FER^{ECD} was determined by MR using the structure of FER^{ECD}. The crystal structure of LLG1 was determined by MR using the coordinates of LLG2 from the structure of RALF23-LLG2-FER^{ECD}. All the models were built with the program COOT[27] and subsequently subjected to refinement by the program Phenix[28] with excellent stereochemistry (Extended Data Table 1). Structural figures were prepared using the program PyMOL.

Isothermal titration calorimetry

Binding affinities were measured using ITC200 (Microcal LLC) at 25 °C in a buffer containing 10 mM Bis-Tris, pH6.0 and 100 mM NaCl. Ligands (approximately 0.5 mM) were injected (20 × 2.0 μL) at 150 s intervals into the stirred (750 rpm) calorimeter cell (volume 250 μL) containing 0.05 mM receptors. Measurements of the binding affinity of all the titration data were analysed using the ORIGIN 7 software (MicroCal Software).

Sedimentation-velocity analytical ultracentrifugation.

Sedimentation velocity was measured for FER^{ECD} and LLG1/2/3 in the presence or absence of chemically synthesized RALF peptides with an XL-I analytical ultracentrifuge (Beckman Coulter) equipped with an eight-cell An-50 Ti rotor at 20℃.

The molar ratio in the mixture solution of FER^{ECD}:LLG1/2/3:RALF peptide and the total OD_{280} were approximately 1:2:3, and 0.8, respectively. Buffer (10 mM Bis-Tris pH 6.0, 100 mM NaCl) was used as the reference solution. All samples were applied at a speed of 50,000 rpm. Absorbance scans were taken at 280 nm at the intervals of 0.003 cm size in a radical direction. The different sedimentation coefficients, c(s), and molecular weight were calculated by SEDFIT V14.4f software.

Surface plasmon resonance

The surface plasmon resonance experiment was performed using a BIACORE T200 instrument (GE Healthcare) on a CM5 sensor chip captured with anti-histidine antibodies (His Capture Kit, GE Healthcare) through standard amine-coupling chemistry. C-terminal-histidine-tagged LLG2 at a concentration of 50 µg/mL was immobilized at a density of 700 RU on flow cell 2 and flow cell 1 was left blank to serve as a reference surface for the following experiments. The analyte, RALF23-17mer (residues 1-17), was injected over the two flow cells. The sensorgram represents binding of the peptide in the analyte concentration range (50 - 800 nM), where dissociation was initiated by the washing buffer. All experiments were performed in 1xPBS pH 7.5, 0.05% Tween-20, 0.1% BSA at temperature of 25°C. The obtained data were analysed and fitted using the Biocore T200 Evaluation Software and simple one-to-one interaction model.

Pull-down assays

Purified GST-tagged RALF23-17mer (residues 1-17) (GST-17mer) proteins or 17mer mutants were mixed with excess WT or mutant LLG2 and incubated with 100 µL GST resin (GE Healthcare / GS4B) on ice for 30 min after sufficient agitation. The resin was washed with 1.0 mL buffer containing 25 mM Tris pH 8.0, 150 mM NaCl, 15 mM imidazole for three times, and bound proteins were eluted from resin by addition of 50 µL SDS loading buffer at 100 °C for 5 min. Proteins were separated by SDS-PAGE and detected by Coomassie blue staining.

Microscale thermophoresis assays.

FER^{ECD} was labelled with a fluorescent dye using a labelling kit (MO-L001 Monolith™ Protein Labelling Kit RED-NHS (Amine Reactive). Fluorescently-labelled FER^{ECD} (0.052 µM) was mixed with varying peptide concentrations (ranging from 0.009 to 30

492 μM) in buffer containing 50 mM NaH_2PO_4/Na_2HPO_4 pH 7.5, 200 mM NaCl, 5%
493 Glycerol and 0.001% Tween. Approximately 4-6 μL of each sample was loaded in a
494 fused silica capillary (NanoTemper Technologies). Measurements were performed at
495 room temperature in a Monolith NT.115 instrument at a constant LED power of 30%
496 and varying MST power of 20%, 40% and 60%. Measurements were performed
497 repeatedly on independent protein preparations to ensure reproducibility. The data
498 were analysed by plotting peptide concentrations against ligand-induced
499 fluorescence changes (Δ Raw Fluorescence on y axis). Curve fitting was performed
500 by using the Prism 7 (GraphPad Software) and the given KDs were calculated with
501 95% confidence level.

502 **Plant material and growth conditions**

503 Arabidopsis ecotype Columbia (Col-0) was used as a wild type control for all plant
504 assays. Plants for ROS burst assays were grown in individual pots at 20-21 °C with
505 an 8 h-photoperiod in environmentally controlled growth rooms. Seeds for seedling-
506 based assays were surface sterilized using chlorine gas for 6 h and grown on
507 Murashige and Skoog (MS) media supplemented with vitamins, 1% sucrose and
508 0.8% agar at 22 °C and a 16 h-photoperiod. The *fer-2* mutant[29] was kindly provided
509 by Nana Keinath (University of Heidelberg). The *fer-4, llg1-1, llg1-2* and *llg1-3* were
510 recently published[11,12,30], and kindly provided by Alice Cheung (University of
511 Massachusetts) and Dingzhong Tang (Fujian Agriculture and Forestry University),
512 respectively.

513 **ROS burst measurement**

514 Eight leaf discs (4 mm in diameter) per individual genotype were collected in 96-well
515 plates containing sterile water. After collection, leaf discs were recovered over night
516 before elicitor treatment. The next day, the water was replaced by a solution
517 containing 17 μg/mL luminol (Sigma Aldrich), 20 μg/mL horseradish peroxidase (HRP,
518 Sigma Aldrich) and the PAMP in the appropriate concentration. Luminescence was
519 measured for the indicated time period using a charge-coupled device camera
520 (Photek Ltd., East Sussex UK).

521 The effect of RALF23 on elf18-triggered ROS production was performed as
522 previously described[5] .

RALF-induced seedling growth inhibition

Seeds were surface-sterilized and grown on MS Agar plates for 5 days before transferring individual seedlings in each well of a 48-well plate containing MS medium with 500 nM or 1 µM RALF23 or RALF23 mutant variant. Seedling growth was measured 7 days after transfer.

Co-immunoprecipitation and Western blots

FLS2-BAK1 complex formation experiments were performed as previously described[5]. To test the *in vivo* interaction between LLG1 and FER, fifteen to twenty seedlings of *llg1-3* 35S::YFP-LLG1[12] were grown in 6-well plates for 2 weeks, transferred to 2 mM MES-KOH, pH 5.8 and treated with 1 µM RALF23 for 10 minutes. Seedlings were than frozen in liquid nitrogen. Proteins were extracted in 20 mM MES-KOH pH 6.3, 50 mM NaCl, 10% glycerol, 5 mM dithiothreitol, 1% protease inhibitor cocktail (Sigma Aldrich), 2 mM Na_2MoO_4, 2.5 mM NaF, 1.5 mM activated Na_3VO_4, 1 mM phenylmethanesulfonyl fluoride and 1 % IGEPAL. For immunoprecipitations GFP-Trap agarose beads (ChromoTek) were used and incubated with the crude extract for 2-3 h at 4° C. Beads were then washed 3 times with 20 mM MES-KOH pH 6.3, 50 mM NaCl, 1 mM phenylmethanesulfonyl fluoride, 0.1 % IGEPAL before adding Laemmli sample buffer and incubating for 10 min at 95° C. Eluted proteins were analysed by western blot using α-FER and α-GFP (B-2 HRP, sc-9996, Santa Cruz, used at 1:5,000). The α-FER antibody was raised against two synthetic peptides corresponding to the ectodomain of FER (CEDSKTSPALTQDPSV and CPSADTGLYRSWYDDQ) by Eurogentec (Belgium), and was detected using anti-rabbit IgG-HRP secondary (A0545, Sigma, used at 1:5,000). Specificity of α-FER was validated using *fer-4* knockout plants (Extended data Fig. 2e).

For assays using transient heterologous expression, leaves of 4.5-week-old *N. benthamiana* plants were co-infiltrated with *Agrobacterium tumefaciens* carrying 35S::FER-GFP and 35S::SP-mRFP-LLG1 (WT or point mutant) constructs. In all cases constructs were also co-infiltrated with a P19 silencing suppressor construct. Leaves were harvested 2 days post-infiltration and equilibrated in 2 mM MES-KOH pH 5.8 (via vacuum infiltration) for 2-3 hours. Leaves were then treated with mock or 5 µM RALF23 peptide for 10 minutes before freezing in liquid nitrogen. Protein

554 extraction, immunoprecipitation, and Western blotting were performed as above. SP-
555 mRFP-LLG1 proteins were detected with α-RFP (ab34767, Abcam, used 1:5,000).

556 **Generation of FER and LLG1 structure-guided point mutants**

557 *FER* wild-type sequence was amplified from *Arabidopsis* seedling cDNA using
558 primers CACCATGAAGATCACAGAGGGACGATTC
559 and ACGTCCCTTTGGATTCATGATCTGAG before cloning into pENTR (Invitrogen)
560 using the D-TOPO kit (Invitrogen). Structure-guided point mutants FER^{G257A} and
561 FER^{N303Y} were introduced by site-directed mutagenesis PCR using the following
562 primers: G257A-F: CAGCCTTATATATTTGCTGCAGGACTTGGTATTCC
563 G257A-R: GGAATACCAAGTCCTGCAGCAAATATATAAGGCTG

564 N303Y-F: GCTCAGATCAATCTCTACTACAATCTTACTTGG

565 N303Y-R:CCAAGTAAGATTGTAGTAGAGATTGATCTGAGC

566 To drive expression of FER-GFP under the native FER promoter (pFER), 2,004 bp
567 upstream of the *FER* start codon were amplified from seedling cDNA using primers
568 GGCCAGTGCCAAGCTTCGAGTTGTAAAAGGCCTGG
569 and GCAGGCATGCAAGCTTCGATCAAGAGCACTTCTCC for subsequent cloning
570 into Gateway destination vector pGWB404[31] using Infusion cloning (Takara Bio) and
571 the HindIII restriction enzyme (Thermo Scientific). The LR Clonase II kit (Invitrogen)
572 was used to recombine pENTR-FER and the respective point mutants with the
573 pGWB404-pFER vector. Expression of the constructs in independent transgenic *fer-4*
574 lines was tested by western blot using α-GFP antibodies (Santa Cruz biotechnology).
575 To generate FER-GFP fusion constructs for transient expression in *Nicotiana*
576 *benthamiana* and co-immunoprecipitation experiments, pENTR-FER was recombined
577 with pK7FWG2 (VIB Ghent) using LR clonase (Invitrogen. To generate LLG1 and
578 structure-guided point mutants for transient *Nicotiana benthamiana* protein
579 expression and co-immunoprecipitation experiments, signal peptide (SP)-mRFP-
580 LLG1 constructs (WT, N91A, T99R, A117Y and N118Y) were obtained by gene
581 synthesis (Twist Bioscience). The mRFP sequence was inserted after the first 78 bp
582 of the LLG1 CDS encoding for the signal peptide, followed by the downstream 429
583 bp of LLG1. Constructs were flanked at 5` and 3` ends with attB attachment sites
584 allowing subsequent BP cloning into the gateway entry vector pDONR/Zeo
585 (Invitrogen). Subsequently, pDONR/Zeo SP-mRFP-LLG1 constructs were

recombined with pGWB402[31] destination vectors using LR clonase (Invitrogen) for in planta expression under control of the CaMV 35S promoter.

Statistical analysis

Statistical significance was assessed applying one-way ANOVA analysis using Prism 6.0 (GraphPad Software).

Reporting Summary

Further information on research design is available in the Nature Research Reporting Summary linked to this paper.

Data availability

The atomic coordinates and structure factors have been deposited in the Protein Data Bank (PDB). The PDB codes of $ANX1^{ECD}$, FER^{ECD}, $ANX2^{ECD}$, LLG1 RALF23-LLG2-FER^{ECD} structures are 6A5A, 6A5B, 6A5C, 6A5D, 6A5E, respectively. For gel source images, see Supplementary Figs 1-3. All other data or materials can be obtained from the corresponding author upon request.

5 Stegmann, M. *et al.* The receptor kinase FER is a RALF-regulated scaffold controlling plant immune signaling. *Science* **355**, 287-289 (2017).

11 Li, C. *et al.* Glycosylphosphatidylinositol-anchored proteins as chaperones and co-receptors for FERONIA receptor kinase signaling in Arabidopsis. *Elife* **4** (2015).

12 Shen, Q., Bourdais, G., Pan, H., Robatzek, S. & Tang, D. Arabidopsis glycosylphosphatidylinositol-anchored protein LLG1 associates with and modulates FLS2 to regulate innate immunity. *Proc. Natl. Acad. Sci. U. S. A.* **114**, 5749-5754 (2017).

24 Wang, Q. S. *et al.* Upgrade of macromolecular crystallography beamline BL17U1 at SSRF. *Nuclear Science & Techniques* **29**, 68 (2018).

25 Otwinowski, Z. & Minor, W. Processing of X-ray diffraction data collected in oscillation mode. *Macromolecular Crystallography, Pt A* **276**, 307-326 (1997).

26 McCoy, A. J. *et al.* Phaser crystallographic software. *Journal of Applied Crystallography* **40**, 658-674 (2007).

27 Emsley, P. & Cowtan, K. Coot: model-building tools for molecular graphics. *Acta Crystallographica Section D-Biological Crystallography* **60**, 2126-2132 (2004).

28 Adams, P. D. *et al.* PHENIX: Building new software for automated crystallographic structure determination. *Acta Crystallographica Section D Biological Crystallography* **58**, 1948-1954 (2002).

29 Deslauriers, S. D. & Larsen, P. B. FERONIA is a key modulator of brassinosteroid and ethylene responsiveness in Arabidopsis hypocotyls. *Mol. Plant* **3**, 626-640 (2010).

30 Duan, Q., Kita, D., Li, C., Cheung, A. Y. & Wu, H. M. FERONIA receptor-like kinase regulates RHO GTPase signaling of root hair development. *Proc. Natl. Acad. Sci. U. S. A.* **107**, 17821-17826 (2010).

31 Nakagawa, T. *et al.* Improved Gateway binary vectors: high-performance vectors for creation of fusion constructs in transgenic analysis of plants. *Biosci. Biotechnol. Biochem.* **71**, 2095-2100 (2007).

Acknowledgments

We thank J. He at Shanghai Synchrotron Radiation Facility (SSRF) and G. Lin for assistance with X-ray diffraction data collection, and C. Zhou at Tsinghua University Branch of China National Center for Protein Sciences Beijing for assistance with SV-AUC data collection and analysis, as well as Ivan Hang from the Vienna Biocenter Core Facilities and Y. Zhu, S. Liu from Tsinghua University for help with protein purification. We thank R. Hückelhoven, Technical University Munich, in whose department part of the work was performed. The SPR equipment was kindly provided by the EQ-BOKU VIBT GmbH and the BOKU Core Facility for *Biomolecular and Cellular Analysis*.This research was funded by Projects of International Cooperation and Exchanges NSFC (31420103906), Chinese Ministry of Science and Technology (2015CB910200) and National Natural Science Foundation of China (31421001) (J.C.), the Gatsby Charitable Foundation (C.Z.), the University of Zürich (C.Z.), the European Research Council under the Grant Agreements 309858 and 773153 (grants "PHOSPHinnATE" and "IMMUNO-PEPTALK" to C.Z.), the Deutsche Forschungsgemeinschaft (Fellowship STE 2448/1 to M.S.), the Technical University of Munich (M.S.), the European Molecular Biology Organization (EMBO Long-Term Fellowship 100-2017 to T.A.D.), and the Austrian Academy of Science through the Gregor Mendel Institute (Y.B). K.Parys was supported by the Vienna Science and Technology Fund Project (LS17-047).

Author contributions

J. Chai, C. Zipfel, Y. Xiao and M. Stegmann designed the project. J. Chai and C. Zipfel supervised the project. Y. Xiao and Z. Han performed protein expression and purification, crystallization, X-ray diffraction data collection and processing, ITC assays, SV-AUC assays and pull-down assays. J. Chai and Y. Xiao determined the structures. M. Stegmann and T. DeFalco performed the physiological and biochemical plant assays. K. Parys performed MST and SPR assays under Y.

Belkhadir supervision. Y. Xiao and L. Xu performed LLG1/2 crystallization assays. The data were analyzed by all the authors. J. Chai, C. Zipfel and Y. Xiao wrote the manuscript with input from all the authors.

Competing interests

The authors declare no competing interests.

Extended Data Figure legends

Extended Data Figure 1 | Loss of *LLG1* phenocopies *fer* in flg22-triggered FLS2-BAK1 complex formation and ROS production.

a Tissue-specific expression patterns of *FER* (AT3G51550), *LLG1* (AT5G56170), *LLG2* (AT2G20700) and *LLG3* (AT4G28280) were obtained using Genevestigator (www.genevestigator.com) and are based on the AT_mRNASeq_ARABI_GL-1 data set. *FER* is ubiquitously expressed throughout most tissues, including leaves. Similarly, *LLG1* shows strong expression in vegetative tissue, unlike *LLG2* and *LLG3*, which are predominantly expressed in reproductive tissue. All assays in this study were performed using seedlings or leaf tissue. *LLG1/2/3* expression in these tissues is highlighted by a black box.

b Loss of *LLG1* results in reduced flg22-triggered ROS production. ROS burst was measured in leaf discs of the indicated genotypes after elicitation with 100 nM flg22. Values are represented as total photon counts over 40 min. Biologically independent leaf discs: n=8 for all genotypes +/- SEM. Letters indicate the result of a post hoc turkey test. Columns with same letters are statistically indistinguishable (>95% confidence). See supplementary statistical information for multiple comparison p-values. The experiments were repeated at least three times with similar results

c *LLG1* contributes to flg22-induced FLS2-BAK1 complex formation. *Arabidopsis* Col-0, *fer-2* or *llg1-2* seedlings were treated with 100 nM flg22 for 10 min before immunoprecipitating FLS2. Western blots for protein detection were probed with α-FLS2 and α-BAK1 antibodies. The experiments were repeated at least three times with similar results. See Supplementary Fig. 1 for gel source data,

Extended Data Figure 2 | RALF23 induces LLG2/3 interaction with FER *in vitro*.

a **-b** Quantification of the binding affinities of RALF23 with LLG2/3 or LLG2/3 with FER^{ECD} by ITC. The assays were performed as described in Fig. **1e**.

c **-d** Analyses of and LLG2/3+FER^{ECD} and RALF23+LLG2/3+FER^{ECD} (right) proteins by sedimentation-velocity analytical ultracentrifugation (SV-AUC). The assays were as described in Fig. **1d**

e Analysis of the α-FER antibody. The α-FER antibody was raised against two peptides derived from the extracellular domain of FER in rabbits by Eurogentec (Belgium). The specificity of the antibody was tested by probing samples of Col-0, *fer-4* and *fer-4*/FER-GFP seedling crude protein extract. A specific band for FER in Col-0 migrating between 100 and 130 kDa was detected, which was absent in *fer-4* mutants. Furthermore, a shifted band migrating at a higher molecular weight was detected in *fer-4*/FER-GFP, corresponding to the size increase by the addition of the GFP fusion tag. The experiments were repeated at least three times with similar results. See Supplementary Fig. 1 for gel source data,

Extended Data Figure 3 | Structure of RALF23-LLG2-FER^{ECD} complex.

a The 2Fo-Fc electron density map (blue mesh) of the finally refined RALF23-LLG2-FER^{ECD} model contoured at 1.2σ (under COOT) shown in two orientations. The two RALF23-LLG2-FER^{ECD} molecules in an asymmetric unit are shown in yellow.

b Crystal packing of RALF23-LLG2-FER^{ECD} in the P1 space group shown in two orientations. Colour codes are indicated.

c A stereo view of the structure of RALF23-LLG2-FER^{ECD}

d The 2Fo-Fc electron density map (blue mesh) of the finally refined model contoured at 1.2σ (under COOT) shows glycosylation of Asn142, Asn305 and Asn345 of FER^{ECD} (NAG, N-acetyl-D-glucosamine).

e The 2Fo-Fc electron density map (blue mesh) contoured at 1.2σ (under COOT) shows glycosylation of Asn52 of LLG2.

f Mapping of the glycosylation sites on the structure of RALF23-LLG2-FER^{ECD} Colour codes and the glycosylated residues are indicated.

Extended Data Figure 4 | Structural superposition of apo-FER^{ECD} with apo-ANX1/2^{ECD}, malectin-nigerose (NGR) complex from *Xenopus laevis* and some details in the structure of RALF23-LLG2-FER^{ECD} complex.

a Structural superposition of apo-FER^{ECD} (cyan) apo-ANX1^{ECD} (blue) and apo-ANX2^{ECD} (green). Structural alignment of apo-ANX1$^{ECD\ (26\text{-}410)}$ or apo-ANX2$^{ECD\ (27\text{-}414)}$ with apo-FER$^{ECD\ (29\text{-}423)}$ with r.m.s.d. 0.876 and 0.754 Å, respectively. α3 and

β16 are labeled.

b Structural comparison of the malectin domains of FER^{ECD} (cyan/light blue) with malectin-NGR (gray-yellow) complex from *Xenopus laevis* (PDB code: 2k46). Malectin B of FER (residues 197-447) is used as the template for alignment with malectin A of FER (residues 27-196) with an r.m.s.d. 4.065 Å, and with MALECTIN (residues 1-190) with an r.m.s.d. 16.157 Å. Black box and arrow show the LLG2 binding region in malectin B of FER^{ECD}. The red box marks the NGR binding pocket of malectin-NGR.

c Saccharide recognizing residues are not conserved among malectins. Sequence alignment of malectin domain A, B from FER and malectin from *Xenopus laevis*. Red dots mark residues forming a NGR-perception pocket in malectin.

d Structural superposition of $FER^{ECD\ (29\text{-}423)}$ and RALF23-LLG2-$FER^{ECD\ (29\text{-}423)}$ with an r.m.s.d. (root mean square difference) 0.441 Å. Colour codes are indicated.

e The N-terminal region (residues 4-17, brown) of RALF23 binds to a surface groove of LLG2 (shown in electrostatics). Important residues of RALF23 recognized by LLG2 are indicated.

f The 2Fo-Fc electron density map (blue mesh) around the N-terminal region of RALF23 (residues 4-17) in the finally refined model contoured at 1.2σ (under COOT). The structural model of the N-terminal region is highlighted within the dashed cyan frame, and the LLG2-interacting residues are labelled in white.

g FER^{ECD} (cartoon, cyan) interacts with both LLG2 (surface, purple) and RALF23 (surface, brown). Some secondary structures of FER^{ECD} are indicated (α: α-helix, β: β-sheet).

Extended Data Figure 5 | Structure based sequence alignment of CrRLK1L family in their extracellular domains

Secondary structure elements in FER^{ECD} are marked above. The regions related to RALF23-LLG2-FER^{ECD} interaction are boxed with dashed lines. The important amino acids of FER for interaction with RALF23 or LLG2 are marked with blue dots.

Extended Data Figure 6 | RALF23-17mer is sufficient to induce LLG1/2/3-FER^{ECD} interaction and RALF23 (18-50) reinforces RALF23-LLG1/2/3-FER^{ECD} complex *in vitro*.

a Top panel: SPR sensorgram for the LLG2-RALF23^{N} binding analyses with the corresponding association (ka) and dissociation (kd) rate constant and dissociation constants K_D. Multi-cycle kinetics was used to validate the interaction. The analyte was injected in a concentration range 50-800 nM. The sensorgram presents curves after background subtraction (Fc 2-1). Bottom panel: steady‑state curve fitting analysis for LLG2-RALF23^{N} interaction was used for K_D calculation. The assays were performed three times independently with similar results

b -e Quantification of the binding affinities of different RALF23 variants with LLG1/2/3 by ITC. The assays were performed three times independently with similar results as described in Fig. **1e**. Excessive RALF23-17mer was pre-incubated with LLG1/2/3 for quantification of interaction with FER^{ECD}, whereas excessive LLG1/2/3 was incubated with RALF23 for interaction with FER^{ECD}.

Extended Data Figure 7 | LLG2 interacts with RALF peptides from subfamily 1 but not with subfamily 2.

a Full-length RALF23 is required for biological activity. Five day-old Col-0 seedlings were treated with 1 µM RALF23, 1 µM RALF23 17-mer (RALF23^{N}) or RALF23 residues 18-50 (RALF23^{C}) for 7 days before measuring fresh weight. Shown is the relative fresh weight of seedlings compared to the MS control. Biologically independent seedlings: n=12 for all genotypes +/-SD. Letters indicate the result of a post hoc turkey test. Columns with same letters are statistically indistinguishable (>95% confidence). See supplementary statistical information for multiple comparison p-values. The experiments were repeated at least three times with similar results

b N-terminal sequence alignment of mature RALFs (subfamily 1) from Arabidopsis. Conserved or similar residues are boxed with red background or shown in red font, respectively.

c Summary of the sequences of the RALF peptides used.

d Quantification of LLG2 interaction with RALF peptides from subfamily 1 by ITC. The calculated stoichiometries (n) and the dissociation constants (K_d) are indicated. The assays were performed three times independently with similar results as described in Fig. **1e**.

e N-terminal sequence alignment of RALFs (subfamily 2) from *Arabidopsis*. Conserved and similar residues are boxed in blue and shown in red font, respectively.

f Quantification of RALF11/12/13-22mer or RALF21-16mer interaction with LLG2 by ITC. The calculated stoichiometries (n) and the dissociation constants (K_d) are indicated. The assays were performed three times independently with similar results as described in Fig. **1e**.

Extended Data Figure 8 | Structure-based sequence alignment of the *Arabidopsis* LRE/LLG family and RALFs in subfamily 1 induce LLG1-FER^{ECD} interaction *in vitro*.

a Analyses of proteins indicated by SV-AUC. The assays were performed three times independently with similar results as described in Fig. 1**d**. The profiles of SV-AUV for RALF1/4/14/19/34 + LLG1 + FER^{ECD} are shown in cyan.

b Sequence alignment of LLG1/2/3 and LRE from Arabidopsis. Secondary structure elements in apo-LLG1 are marked on the top. Four pairs of disulfide bonds are labelled underneath in green. The signal peptide, conformationally flexible region and GPI-anchor region are coloured as indicated. The conserved amino acids involved in LLG1/2/3 interaction with RALF23 are marked below the alignment with dots and the non-conserved Arg120 of LRE are marked below the alignment with black dot specially.

c Analyses of proteins indicated by SV-AUC. The assays were performed three times independently with similar results as described in Fig. 1**d**. The profiles of SV-AUV for RALF23 + LRE + FER^{ECD} are shown in cyan.

Extended Data Figure 9 | Mutagenesis analysis of RALF23-LLG1/2-FER^{ECD} interaction

a Quantification of RALF23 binding to LLG1 G114R indicated by ITC.

b Mutagenesis analyses of GST-RALF23-17mer (GST-17mer) interaction with LLG2 by the assays described in Fig. **4c**. Left panel: SDS-PAGE of LLG2 pulled down by wild type or GST-17mer mutants indicated. Right panel: SDS-PAGE of wild type or LLG2 mutants pulled down by GST-17mer. See Supplementary Fig. 2 for gel source data,

c Quantification of RALF23-17mer+LLG1 N118Y binding to FER^{ECD}, and RALF23-17mer+LLG1 binding to the four FER mutants indicated by ITC.

d Quantification of binding of RALF23-17mer +LLG2 to the FER mutants indicated.

e Summary of ITC results on RALF23-17mer+LLG2 interaction with wild type or mutant FER^{ECD}.

f Expression analysis of pFER::FER-GFP and the respective point mutants in the *fer-4* mutant background. Western blots for protein detection were probed with α-GFP antibodies. CBB coomassie brilliant blue. See Supplementary Fig. 1 for gel source data,

g Structure-guided LLG1 mutants disrupt the RALF23-induced complex with FER *in vivo*. *N. benthamiana* leaves co-expressing FER-GFP and SP-mRFP-LLG1 (WT or mutant variants as indicated) were treated with buffer with or without 5 μM RALF23 for 10 min before immunoprecipitation. Experiments were repeated at least three times with similar results. See Supplementary Fig. 3 for gel source data,

Extended Data Table legends

Extended Data Table 1 | Summary of crystallography analyses.

Rsym = $\Sigma h\ \Sigma i|Ih,i - Ih|/\Sigma h\ \Sigma i\ Ih,i$, where Ih is the mean intensity of the i observations of symmetry related reflections of h. R = $\Sigma|Fobs - Fcalc|/\Sigma Fobs$, where $Fobs = FP$, and $Fcalc$ is the calculated protein structure factor from the atomic model. R.m.s.d. in bond lengths and angles are the deviations from ideal values.

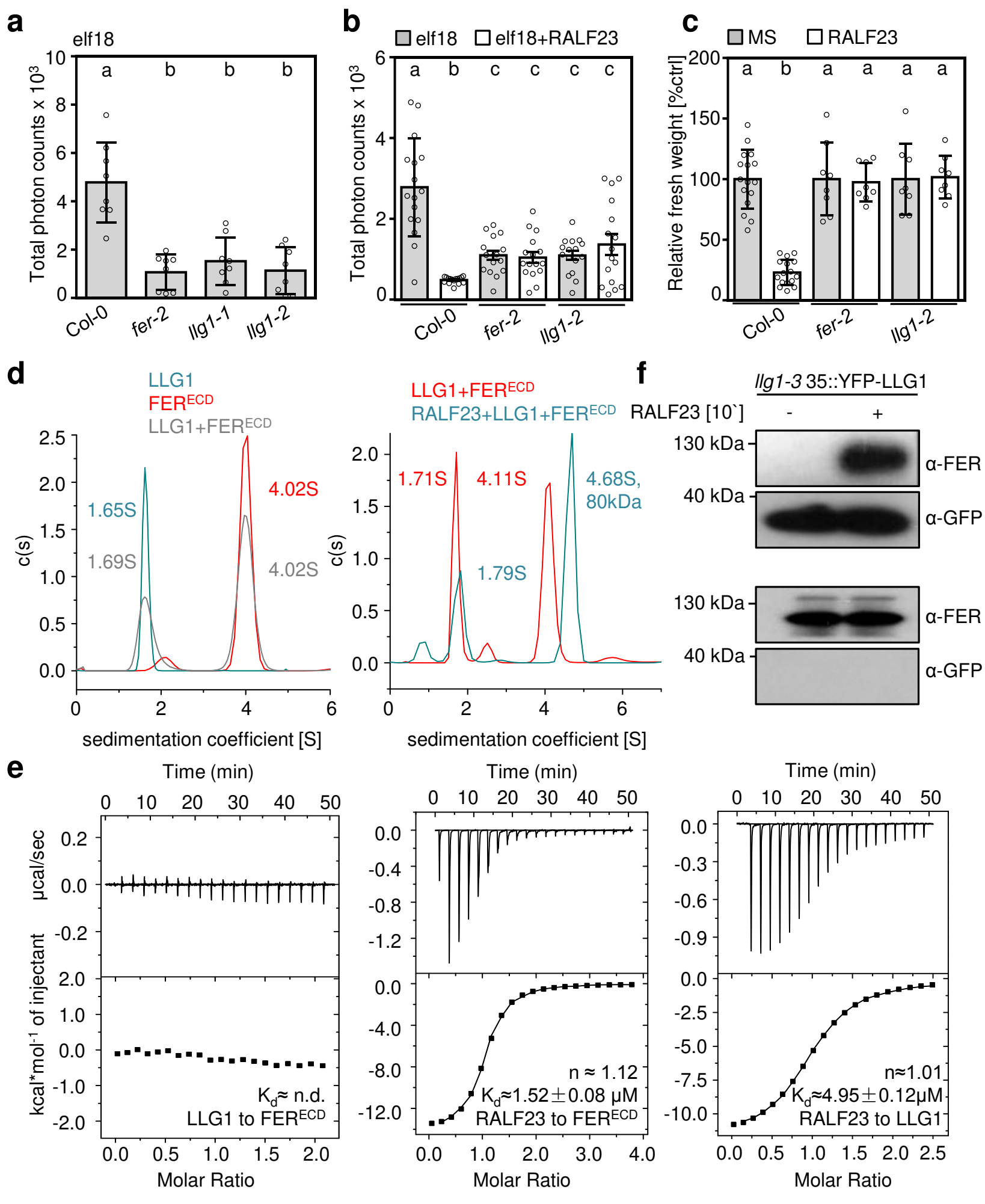
a
elf18
Total photon counts x 10³
a b b b
Col-0
fer-2
llg1-1
llg1-2
b
elf18
elf18+RALF23
Total photon counts x 10³
a b c c c c
Col-0
fer-2
llg1-2
c
MS
RALF23
Relative fresh weight [%ctrl]
a b a a a a
Col-0
fer-2
llg1-2
d
LLG1
FERECD
LLG1+FERECD
1.65S
1.69S
4.02S
4.02S
c(s)
sedimentation coefficient [S]
LLG1+FERECD
RALF23+LLG1+FERECD
1.71S
4.11S
4.68S,
80kDa
1.79S
c(s)
sedimentation coefficient [S]
f
llg1-3 35::YFP-LLG1
RALF23 [10`]
-
+
130 kDa
α-FER
40 kDa
α-GFP
130 kDa
α-FER
40 kDa
α-GFP
e
Time (min)
µcal/sec
kcal*mol-1 of injectant
Kd≈ n.d.
LLG1 to FERECD
Molar Ratio
Time (min)
n ≈ 1.12
Kd≈1.52±0.08 µM
RALF23 to FERECD
Molar Ratio
Time (min)
n≈1.01
Kd≈4.95±0.12µM
RALF23 to LLG1
Molar Ratio

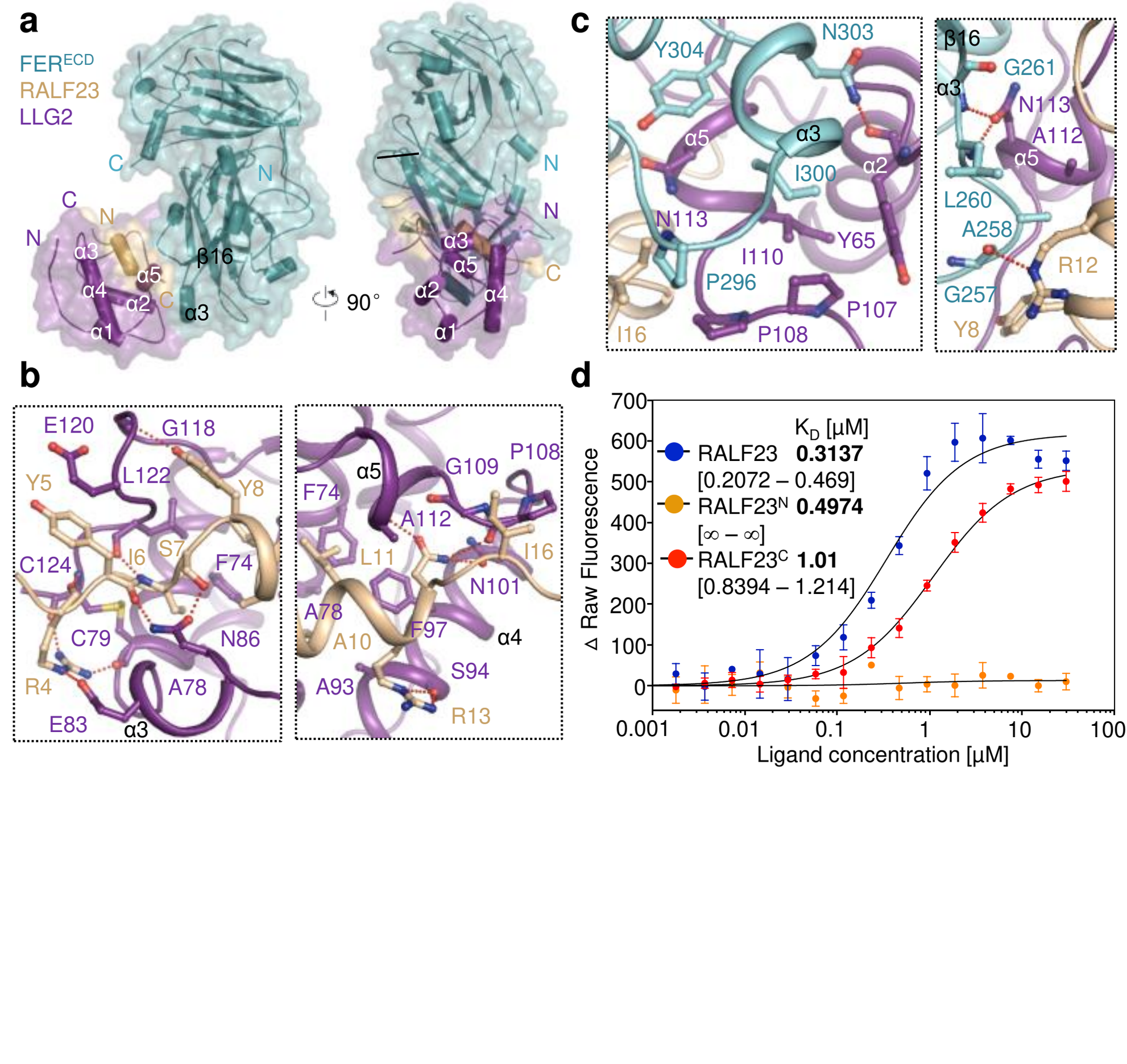
a
FER^ECD
RALF23
LLG2
C
N
C
N
N
α3
β16
α5
α4
α2
C
α3
α1
90°
N
N
C
α3
α5
α2
α4
α1
b
E120
G118
Y5
L122
Y8
C124
I6
S7
F74
C79
N86
R4
A78
E83
α3
α5
G109
P108
F74
A112
L11
I16
N101
A78
A10
F97
α4
S94
A93
R13
c
N303
Y304
α5
α3
I300
α2
N113
Y65
I110
P296
P107
I16
P108
β16
G261
α3
N113
A112
α5
L260
A258
R12
G257
Y8
d
700
600
500
400
300
200
100
0
Δ Raw Fluorescence
K_D [μM]
RALF23 0.3137
[0.2072 – 0.469]
RALF23^N 0.4974
[∞ – ∞]
RALF23^C 1.01
[0.8394 – 1.214]
0.001
0.01
0.1
1
10
100
Ligand concentration [μM]

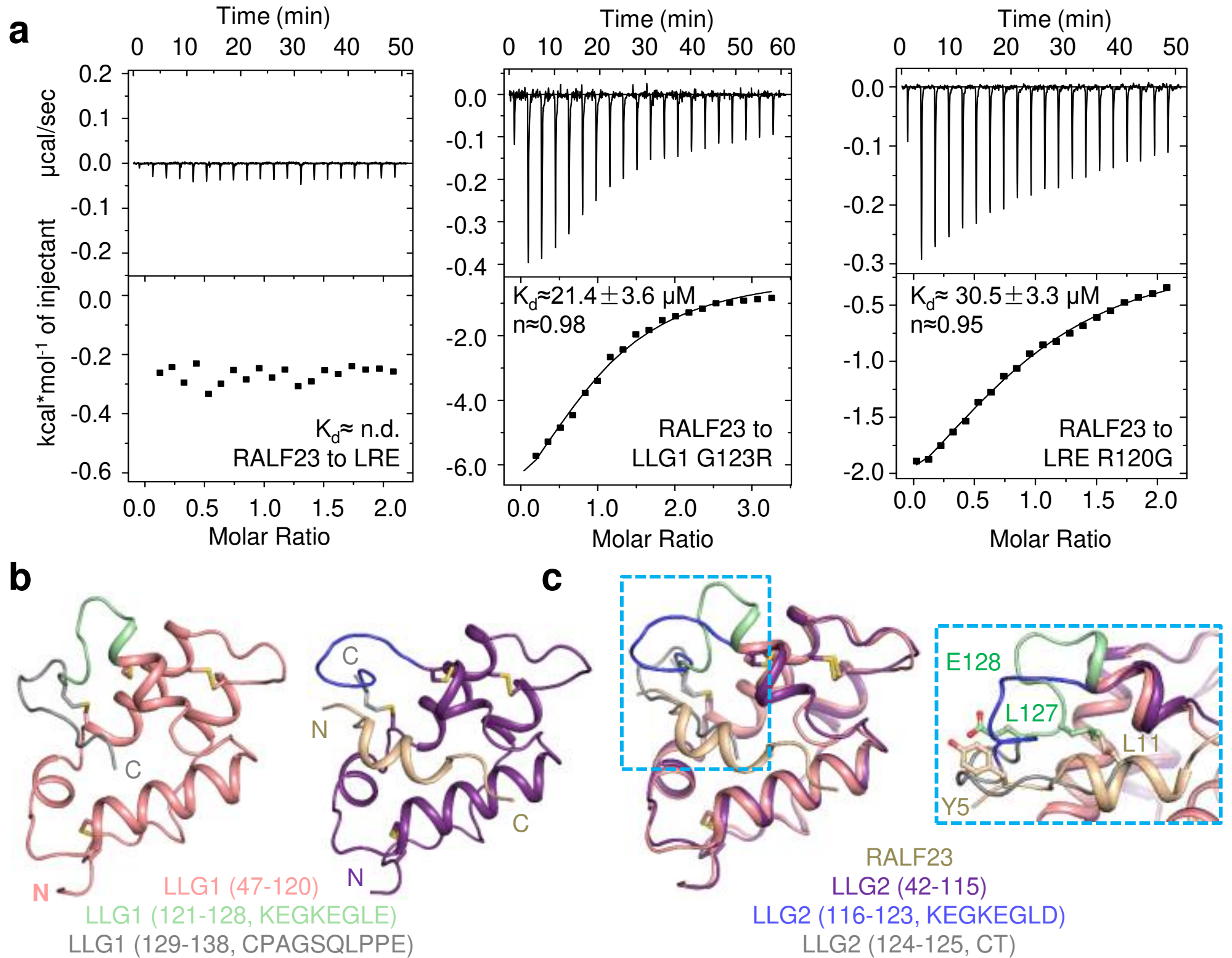
a
Time (min)
µcal/sec
kcal*mol-1 of injectant
Kd≈ n.d.
RALF23 to LRE
Kd≈21.4±3.6 µM
n≈0.98
RALF23 to
LLG1 G123R
Kd≈ 30.5±3.3 µM
n≈0.95
RALF23 to
LRE R120G
Molar Ratio
b
C
N
LLG1 (47-120)
LLG1 (121-128, KEGKEGLE)
LLG1 (129-138, CPAGSQLPPE)
c
E128
L127
L11
Y5
RALF23
LLG2 (42-115)
LLG2 (116-123, KEGKEGLD)
LLG2 (124-125, CT)

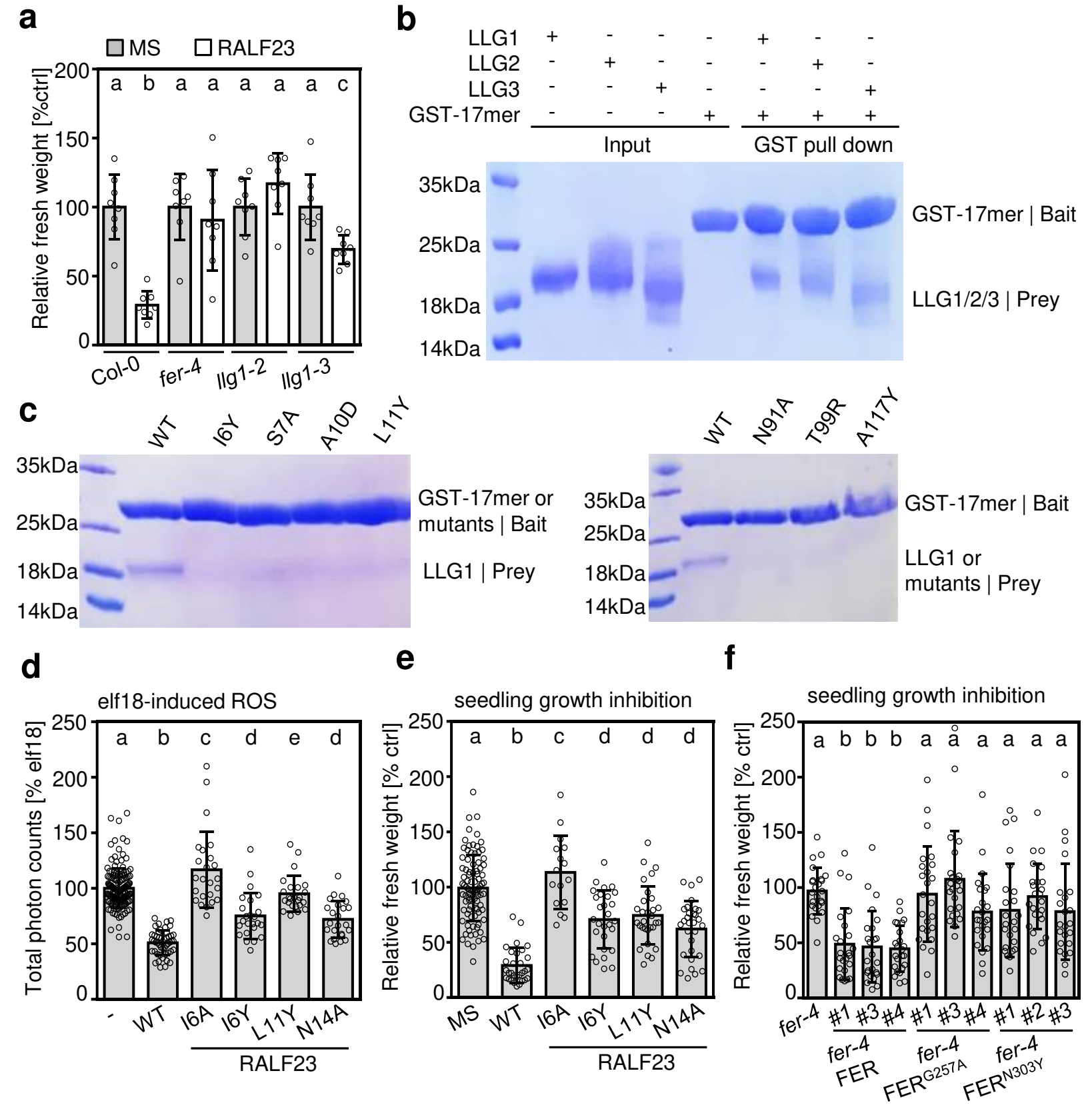
a
MS
RALF23
Relative fresh weight [%ctrl]
200
150
100
50
0
a b a a a a a c
Col-0
fer-4
llg1-2
llg1-3
b
LLG1 + - - - + - -
LLG2 - + - - - + -
LLG3 - - + - - - +
GST-17mer - - - + + + +
Input
GST pull down
35kDa
25kDa
18kDa
14kDa
GST-17mer | Bait
LLG1/2/3 | Prey
c
WT
I6Y
S7A
A10D
L11Y
35kDa
25kDa
18kDa
14kDa
GST-17mer or mutants | Bait
LLG1 | Prey
WT
N91A
T99R
A117Y
35kDa
25kDa
18kDa
14kDa
GST-17mer | Bait
LLG1 or mutants | Prey
d
elf18-induced ROS
Total photon counts [% elf18]
250
200
150
100
50
0
a b c d e d
-
WT
I6A
I6Y
L11Y
N14A
RALF23
e
seedling growth inhibition
Relative fresh weight [% ctrl]
250
200
150
100
50
0
a b c d d d
MS
WT
I6A
I6Y
L11Y
N14A
RALF23
f
seedling growth inhibition
Relative fresh weight [% ctrl]
250
200
150
100
50
0
a b b b a a a a a a
fer-4
#1 #3 #4
fer-4 FER
#1 #3 #4
fer-4 FERG257A
#1 #2 #3
fer-4 FERN303Y